Magnetic reversal in nanoscopic ferromagnetic rings

Kirsten Martens* and D. L. Stein†
Department of Physics, University of Arizona, Tucson, Arizona 85721, USA

A. D. Kent
Department of Physics, New York University, New York, New York 10003, USA
(Received 29 September 2005; revised manuscript received 6 December 2005; published 10 February 2006)

We present a theory of magnetization reversal due to thermal fluctuations in thin submicron-scale rings composed of soft magnetic materials. The magnetization in such geometries is more stable against reversal than that in thin needles and other geometries, where sharp ends or edges can initiate nucleation of a reversed state. The two-dimensional ring geometry also allows us to evaluate the effects of nonlocal magnetostatic forces. We find a "phase transition," which should be experimentally observable, between an Arrhenius and a non-Arrhenius activation regime as magnetic field is varied in a ring of fixed size.

DOI: 10.1103/PhysRevB.73.054413 PACS number(s): 05.40.−a, 02.50.Ey, 75.60.Jk

I. INTRODUCTION

The dynamics of magnetization reversal in submicron-sized, single-domain particles and thin films has attracted much attention given its importance in information storage and other magnetoelectronic applications. The problem can be approached by stochastic methods: in the classical regime (typically at temperatures above ~ 1 K) the magnetization dynamics is governed by the Landau-Lifschitz-Gilbert equation[1] perturbed by weak thermal noise. The classical Néel-Brown theory[2,3] of thermally induced reversal assumed a spatially uniform magnetization and uniaxial anisotropy. Experimental confirmation of this theory has been provided for certain simple single-domain systems (15–30-nm Ni, Co, and Dy nanoparticles).[4]

There, nevertheless, remain fundamental open questions, especially when there is spatial variation of the magnetization density.[5–8] While in small particles that are spherical or nearly so, as in Ref. 4, the Néel-Brown theory appears to work reasonably well, it appears to break down for elongated particles, thin films, and other geometries, which exhibit far lower coercivities than predicted.[9]

Braun[5] made an initial step by studying the effects of spatial variation of magnetization density on magnetic reversal in an infinitely long cylindrical magnet. However, Aharoni[10] pointed out that the energy functional employed neglected important nonlocal magnetostatic energy contributions, invalidating the result. Further, for submicron-scale magnets with large aspect ratio, finite system effects are likely to play an important role; for example, simulations[6,11] indicate that magnetization reversal in cylindrical-shaped particles proceeds via propagation and coalescence of magnetic "end caps," nucleated at the cylinder ends. Both of these issues are addressed in Ref. 12.

Here we consider a geometry that avoids these difficulties: an effectively two-dimensional annulus. Such systems have recently received increasing attention.[13,14] They are typically constructed of soft magnetic materials [quality factor $Q \sim O(10^{-2})$], such as Fe, fcc Co, or permalloy, have radii of order (10^2-10^3) nm and thicknesses of order 10 nm or less.

Our interest in these systems is twofold. The first is technological: because the magnetic bending length is much smaller than the typical system size, there are two oppositely polarized stable states, each with magnetization vectors pointing everywhere along the circumferential direction; they are degenerate in the absence of an external magnetic field. But a current running along the $\hat{\mathbf{z}}$ direction through the center, with $\hat{\mathbf{z}}$ the direction normal to the annulus plane, generates a circumferential magnetic field breaking the degeneracy. By switching the direction of the current, the relative stability of the two states is switched. (A slightly different method, but with similar wire dimensions and current magnitudes, was used in Ref. 13). The utility of such a system as an information storage device depends on the magnetization state being relatively long-lived against thermal fluctuations, even at relatively high temperatures. Unlike the cylindrical particle, the micromagnetic ring has no ends where nucleation is easily initated, making its magnetic state more stable against thermally induced reversal.

The second is physical: by developing a theory for thermally induced reversal that can be solved analytically, we are able to extract a number of interesting qualitative features that would be more difficult to uncover numerically and which should apply also to more complicated situations. While several important quantitative features require a numerical treatment, we show below that our most important qualitative findings are robust (see in particular the Discussion section).

One of our central predictions is that a type of phase transition occurs in the thermally induced reversal rate, and more importantly, that it can be realized experimentally. The possibility of such a transition in classical stochastic field theories (which as we show below includes the physical problem of interest here) was noted in Ref. 15, as system size was varied in a symmetric Ginzburg-Landau double-well ϕ^4 potential. It was further shown in Ref. 16 to apply more generally to asymmetric systems as well. In the present case, the transition depends on *two* parameters: the system size and the strength of the applied magnetic field. Although the former cannot be continuously varied, the latter can, facilitating experimental tests of the predicted transition. In par-

ticular, we will show that as magnetic field varies for a ring of fixed size, there should be a transition from a regime where activation is Arrhenius to one where it is non-Arrhenius. A preliminary account of this work has appeared in Ref. 17.

II. MODEL

We consider an annulus of thickness t, inner radius R_1, and outer radius R_2. We confine our attention to rings satisfying $t \ll \Delta R \ll R$, where $\Delta R = R_2 - R_1$ and $R = (R_1 + R_2)/2$. A current run through the center leads to an applied field $\mathbf{H_e}$ at R in the circumferential direction $\hat{\theta}$; the small variation $\sim O(\Delta R/R)$ of field strength with radius can be ignored. As will be discussed below, magnetostatic forces produce strong anisotropies, forcing the magnetization vector to lie in the plane and preferentially oriented parallel to the inner and outer circumferences. We may therefore consider magnetization configurations that vary only along the $\hat{\theta}$ direction.

Suppose now that the system is initially in its metastable state; i.e., with magnetization vector $\mathbf{M} = -M_0\hat{\theta}$. We are interested in determining the mean rate for thermal fluctuations to reverse the magnetization to its stable direction. We consider temperatures above 1 K, where classical thermal activation can be expected to apply. The magnetization dynamics are then governed by the Landau-Lifshitz-Gilbert equation[1]

$$\partial_t \mathbf{M} = -\gamma[\mathbf{M} \times \mathbf{H}_{\text{eff}}] + (\alpha/M_0)[\mathbf{M} \times \partial_t \mathbf{M}], \tag{1}$$

where M_0 is the (fixed) magnitude of $\mathbf{M}$, α is the damping constant, and $\gamma > 0$ is the gyromagnetic ratio. The effective field $\mathbf{H}_{\text{eff}} = -\delta E/\delta \mathbf{M}$ is the variational derivative of the total energy E, which (with free space permeability $\mu_0 = 1$) is[11,18]

$$E[\mathbf{M}(\mathbf{x})] = \lambda^2 \int_\Omega d^3x |\nabla \mathbf{M}|^2 + \frac{1}{2}\int_{\mathbf{R}^3} d^3x |\nabla U|^2 - \int_\Omega d^3x \mathbf{H}_e \cdot \mathbf{M}, \tag{2}$$

where Ω is the region occupied by the ferromagnet, λ is the exchange length, $|\nabla \mathbf{M}|^2 = (\nabla M_x)^2 + (\nabla M_y)^2 + (\nabla M_z)^2$, and U (defined over all space) satisfies $\nabla \cdot (\nabla U + \mathbf{M}) = 0$. The first term on the right-hand side of Eq. (2) is the bending energy, the second is the magnetostatic energy, and the last is the Zeeman energy. Crystalline anisotropy terms are neglected, given their negligibly small contribution; they can be easily included but will at most result in a small modification of the much larger shape anisotropies, to be discussed below.

III. ENERGY SCALING AND THE MAGNETOSTATIC TERM

The presence of the nonlocal magnetostatic term complicates analysis. However, the quasi-two-dimensional nature of the problem allows a significant simplification, as shown by Kohn and Slastikov[19] in an asymptotic scaling analysis that applies when the aspect ratio $k = t/R$ and the normalized exchange length $l = \lambda/R$ are both small, and $l^2 \sim k|\ln k|$. These constraints restrict the range of ring geometries to which our analysis applies. Before discussing the Kohn-Slastikov (KS) result, we recast the energy in dimensionless form, letting $X = x/R$ and similarly for all other lengths, and let $\mathbf{h} = \mathbf{H}_e/(2M_0 l^2)$. Then, integrating along the direction normal to the plane, we have for the bending plus Zeeman energy contribution

$$\frac{E_b + E_z}{M_0^2 R^3} = kl^2 \int_\omega d^2X [(\nabla_X \mathbf{m})^2 - 2\mathbf{h} \cdot \mathbf{m}], \tag{3}$$

where $\mathbf{m} = \mathbf{M}/M_0$ is the normalized magnetization and ω represents the two-dimensional (2D) surface with boundary $\partial\omega$.

Before analyzing these terms further, we examine the magnetostatic energy contribution. The analysis of Ref. 19 showed that this asymptotically separates into local bulk and surface terms:

$$\frac{E_{\text{mag}}}{M_0^2 R^3} = \frac{1}{2}k\int_\omega d^2X m_z^2 + (1/4\pi)k^2|\ln k| \int_{\partial\omega} ds_X (\mathbf{m} \cdot \hat{\mathbf{r}})^2 + \frac{1}{2}k^2 \int_\omega d^2X |\nabla \cdot \mathbf{m}|^2_{H^{-1/2}}, \tag{4}$$

where s_X is dimensionless arc length along the boundary, and the final integral is the squared $H^{-1/2}$ Sobolev norm of $\nabla \cdot m$.[20] With current technology, the orders of magnitude $k \sim 10^{-2}$ and $l^2 \sim k|\ln k| \sim 10^{-2} - 10^{-1}$ are just attainable. Then the first term of Eq. (4) is larger than the others by roughly two orders of magnitude, forcing $m_z = 0$, and therefore in this topology we can ignore fluctuations of $\mathbf{m}$ out of the plane (we will discuss this further in Sec. III A).

The second term, like the first, is a (local) magnetostatic surface (or shape anisotropy) term. The third term represents a nonlocal magnetostatic bulk energy. When nonzero, this term will be roughly an order of magnitude smaller than the others (see Sec. V B), and so to a first approximation[21] it can be dropped. This will result, for some values of ring size and external field, in an error of up to 10% in the computation of the action, so we can hope at best for reasonably good quantitative predictions of the logarithm of the escape rate. As noted in the Discussion section, however, the important qualitative features uncovered by our analysis should remain unaffected.

We use a locally varying coordinate system where the angle $\phi(s')$ measures the deviation of the local magnetization vector from the local applied field direction; i.e., $\phi = 0$ indicates that the local magnetization is parallel to the local field, $\phi = \pi$ indicates that it is antiparallel, and so on. The parameter $s' = R\theta$ is the arc length along the circumference. The geometry and variables used are displayed in Fig. 1.

The normalized magnetization vector can therefore be written, in cylindrical coordinates, as $\mathbf{m} = (m_r, m_\theta, m_z) = (\sin\phi, \cos\phi, 0)$. After integrating out the radial coordinate the bending plus Zeeman energy becomes

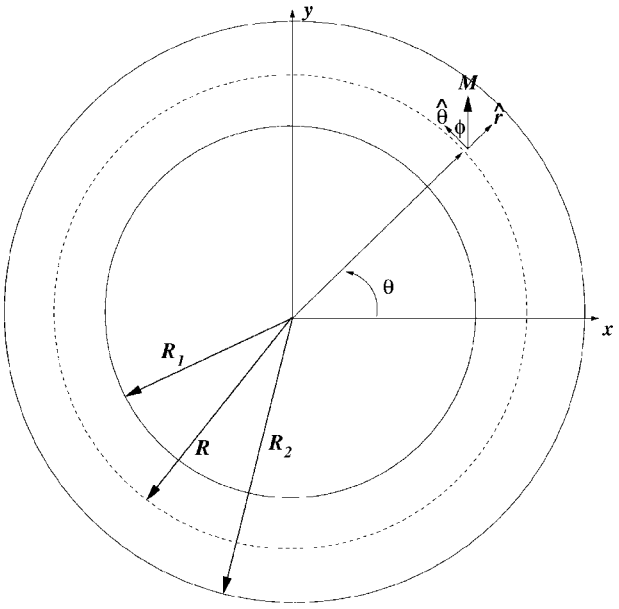

FIG. 1. Ferromagnetic annulus viewed from above, showing coordinates used in text.

$$\frac{E_b+E_z}{M_0^2R^3}=kl^2\left\{\left(\ln\frac{R_2}{R_1}\right)\int_0^{2\pi}d\theta\left[1+\left(\frac{\partial m_r}{\partial\theta}\right)^2+\left(\frac{\partial m_\theta}{\partial\theta}\right)^2+2\left(m_r\frac{\partial m_\theta}{\partial\theta}-m_\theta\frac{\partial m_r}{\partial\theta}\right)\right]-\frac{\Delta R}{R}\int_0^{2\pi}d\theta 2\mathbf{h}\cdot\mathbf{m}\right\}. \tag{5}$$

The $m_r(\partial m_\theta/\partial\theta)-m_\theta(\partial m_r/\partial\theta)$ term is a "winding number" of ϕ with respect to the local direction; it gives zero in all configurations considered here, but would give a nonzero contribution for uniform magnetizations, e.g., $\mathbf{m}=\hat{\mathbf{x}}$. For fixed M_0, it does not contribute to the magnetization equations of motion given by Eq. (1).

Finally, subtracting out constant terms and the first derivative term (which gives zero contribution), noting that the boundary integral occurs over both inner and outer radii, and rescaling lengths again gives

$$\mathcal{E}=\int_0^{\ell/2}ds\left[\left(\frac{\partial\phi}{\partial s}\right)^2+\sin^2\phi-2h\cos\phi\right], \tag{6}$$

where $\mathcal{E}=E/E_0=E/[2M_0^2R^2\Delta R\sqrt{c}kl^2]$, $s=\theta\sqrt{c}$, $\ell=2\pi\sqrt{c}$, $h=|\mathbf{H_e}|/(2M_0l^2c)$, and $c=(1/2\pi)(k|\ln k|/l^2)(R/\Delta R)$. In deriving Eq. (6) we used the fact that $\ln(R_2/R_1)=\Delta R/R+O[(\Delta R/R)^2]$. The error is negligible for the geometries considered here; for example, with the ring parameters used in Fig. 7, $\Delta R/R=1/5$ and $\ln(R_2/R_1)=0.200\,67$. The parameter c $(0<c<\infty)$ depends on the ring size and material properties; it represents the ratio of the anisotropy energy scale to the bending energy scale, and determines the width of a Bloch wall.

A. Energetics and topology

The scaling results of the previous section are useful insofar as they provide results on how different contributions to the energy scale in the thin-film limit. Their effective application in a physical situation must also take into account the geometry, and in our case, the topology of the ferromagnetic particle under study. Consideration of both of these aspects provides a guide for considering what types of magnetization configurations might be relevant in different thin-film geometries.

As one example, we consider the flat disk topology studied by Shinjo *et al.*[22] (corresponding to our geometry with $R_1=0$). They studied magnetization configurations in permalloy disks of thickness 50 nm and diameters ranging from 0.3 to 1 μm. Interestingly, they observed vortex structures, particularly in the larger diameter samples. The surface term energy in Eq. (4) (which leads to the shape anistotropy) is minimized by requiring the magnetization vector to remain tangential to the surface (i.e., in the $\pm\hat{\theta}$ direction). But given the topology of the samples used here, this forces the interior magnetization to do one of two things: either the magnetization *magnitude* goes to zero at the center, or the magnitude stays mostly constant but then the out-of-plane magnetization component $m_z\neq 0$ in some interior region. Either choice costs energy, but (when considered over the same region) the first costs more than the second.

Given that there must be an out-of-plane magnetization component in the disk topology studied by Shinjo *et al.*,[22] the KS analysis can determine the approximate length scale over which this occurs. Comparing the first term in Eq. (4) with the bending term (5), we estimate that their respective energies are of the same order when the region where $m_z\neq 0$ is roughly of the order of an exchange length, i.e., 10–20 nm. This appears to be exactly what is observed. (Shinjo *et al.*[22] do not provide an estimate for the width of this region, noting only that they observe a contrast "spot" at the center of each disk that corresponds to out-of-plane magnetization; see Fig. 2 of their paper.) Note that if the magnetization were to be out of plane in a region much larger than this, Eq. (4) predicts a prohibitively large energy cost. (Simulation results consistent with these conclusions appear in Ref. 23.)

In our ring topology, however, an "outer vortex" configuration (i.e., magnetization circumferential at the outer boundary) does not require an out-of-plane magnetization anywhere. We can therefore ignore configurations with $m_z\neq 0$, any of which are likely to have energies larger than the configurations considered here.

IV. TRANSITION IN ACTIVATION BEHAVIOR

The reversal rate Γ due to thermal fluctuations at temperature T is given by the Kramers formula $\Gamma\sim\Gamma_0\exp(-\Delta W/k_BT)$, where the activation barrier $\Delta W\gg k_BT$ is simply the energy difference between the (meta)stable and "saddle" states. The latter is the state of lowest energy with a single negative eigenvalue (and corresponding unstable direction) of the linearized zero-noise dynamics. Equivalently, it is the configuration of highest energy along the system's optimal escape path.[24] The rate prefactor Γ_0 is determined by fluctuations about this optimal path, and its evaluation will be presented in Sec. V C.

Stable, unstable, and saddle states are all time-independent solutions of the Landau-Lifshitz-Gilbert (LLG) equations. For fixed M_0, Eq. (1) and the variational equation $\mathbf{H}_{\text{eff}}=-\delta E/\delta\mathbf{M}$ yield a nonlinear differential equation that must be satisfied by any such time-independent solution:

$$d^2\phi/ds^2 = \sin\phi\cos\phi + h\sin\phi. \tag{7}$$

There are three "constant" solutions (i.e., ϕ is independent of θ; these remain nonuniform configurations because $\mathbf{m}$ varies with position) for $0\leqslant h<1$: the stable state $\phi=0$ ($\mathbf{m}=\hat{\theta}$); the metastable state $\phi=\pi$ ($\mathbf{m}=-\hat{\theta}$), and a pair of degenerate unstable states $\phi=\cos^{-1}(-h)$, which constitute the saddle for a range of (ℓ,h). The $\phi=0,\pi$ solutions are degenerate when $h=0$, and the $\phi=\pi$ solution becomes unstable at $h=1$. We therefore confine ourselves to fields in the range $0\leqslant h<1$.

We have also found a nonconstant ("instanton") solution[25] of Eq. (7), which we will see is the saddle for the remaining range of (ℓ,h). It is

$$\phi(s,s_0,m) = 2\cot^{-1}\left[\mathrm{dn}\left(\frac{s-s_0}{\delta}\middle|m\right)\frac{\mathrm{sn}(\mathcal{R}|m)}{\mathrm{cn}(\mathcal{R}|m)}\right], \tag{8}$$

where $\mathrm{dn}(\cdot|m)$, $\mathrm{sn}(\cdot|m)$, and $\mathrm{cn}(\cdot|m)$ are the Jacobi elliptic functions with parameter m, $0\leqslant m\leqslant 1$;[26] s_0 is an arbitrary constant arising from the rotational symmetry of the problem; and $\mathcal{R}$ and δ are given by

$$\mathrm{sn}^2(\mathcal{R}|m) = 1/m - h/2 - (1/2m)\sqrt{m^2h^2+4(1-m)}, \tag{9}$$

$$\delta^2 = \frac{m^2}{2-[m+\sqrt{m^2h^2+4(1-m)}]}. \tag{10}$$

The period of the dn function equals $2\mathbf{K}(m)$, the complete elliptic integral of the first kind.[26] Accordingly, imposition of the periodic boundary condition yields a relation between ℓ and m:

$$\ell = 2\mathbf{K}(m)\delta. \tag{11}$$

In the limit $m\to 1$, corresponding to $\ell\to\infty$ at fixed h, Eqs. (8)–(11) reduce to Braun's solution.[5] In the limit $m\to 0$, $\mathrm{dn}(x|0)=1$, and the instanton solution reduces to the constant state $\phi=\cos^{-1}(-h)$. At $m=0$, the critical length and field are related by

$$\ell_c = \pi\delta_c = 2\pi/\sqrt{1-h_c^2}. \tag{12}$$

The solution (8)–(11) corresponds to a pair of domain walls of width $O(\delta)$. At fixed h, the constant configuration is the saddle for $\ell<\ell_c$ and the instanton is the saddle for $\ell>\ell_c$. This can be understood as follows: at fixed field, the bending energy becomes sufficiently large at small ℓ so that the constant state becomes energetically preferred. (There is a second transition at even smaller ℓ, where the bending energy becomes so large that the magnetization lies along a single Euclidean direction everywhere; we do not consider such small length scales here.) Conversely, at fixed ℓ the constant configuration is the saddle for $h>h_c$, and the nonconstant for $h<h_c$. (However, when $\ell\leqslant 2\pi$, the constant configuration is the saddle for all h.) Here the Zeeman term dominates at sufficiently large field, preferring a constant configuration, while at smaller field the shape anisotropy energy dominates, preferring the instanton configuration. The "phase boundary" [Eq. (12)] is the $m=0$ line in the (ℓ,h) plane, and is shown in Fig. 2. We now compute the reversal rate in both regimes, and examine how it is affected by the transition in the saddle state.

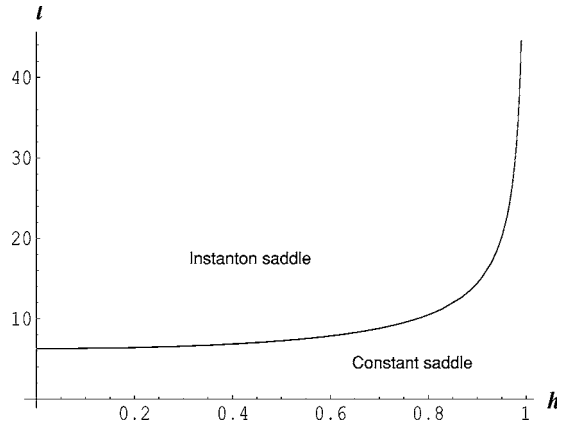

FIG. 2. The phase boundary between the two activation regimes in the (ℓ,h) plane. In the shaded region the instanton state is the saddle configuration; in the unshaded region, the constant state.

V. REVERSAL RATE

We turn now to a computation of the magnetization reversal rate Γ due to thermal fluctuations at temperature T. In equilibrium, it is given, as noted in Sec. IV, by the Kramers formula $\Gamma\sim\Gamma_0\exp(-\Delta W/k_BT)$.[24] We first compute the activation barrier ΔW for each saddle configuration.

A. Activation energy

As noted earlier, the exponential dependence of the magnetization reversal rate on temperature is given by ΔW, the energy difference between the saddle (ϕ_u) and metastable (ϕ_s) states (the notation arises from the properties that the saddle is unstable along the longitudinal escape direction, while the metastable state is locally stable in all directions). With the latter given by $\phi_s=\pi$, this is

$$\begin{aligned}\Delta W/E_0 &= \mathcal{E}[\phi_u]-\mathcal{E}[\phi_s=\pi]\\ &= \int_0^{\ell/2} ds\left[\left(\frac{\partial\phi_u}{\partial s}\right)^2+\sin^2(\phi_u)-4h\cos^2(\phi_u/2)\right].\end{aligned} \tag{13}$$

When the constant state $\phi=\cos^{-1}(-h)$ is the saddle configuration, it easily seen that $\Delta W=(1-h)^2\ell/2$. When the nonconstant, or instanton, state is the saddle, the integral (13) must be computed numerically. However, it can be analytically computed in the $m\to 0$ $[\ell\to\ell_c^+(h)]$ limit, where one finds $\Delta W(m\to 0)\to(1-h)^2\ell/2$. So the energy (and its first derivative, which can also be computed) is continuous at $\ell_c(h)$. Of course, the second derivative is discontinous there.

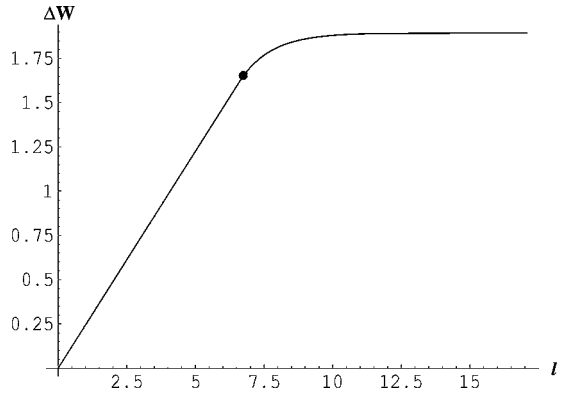

FIG. 3. Activation energy ΔW for fixed $h=0.3$ as ℓ varies. The dot indicates the transition from constant to instanton saddle configuration.

Figure 3 shows the activation energy as a function of ring circumference for fixed field.

The activation energy grows linearly with ℓ when the transition state is constant; it becomes almost flat above ℓ_c at fixed h, because the width of the domain walls remains essentially constant (cf. Fig. 4 of Ref. 16). In Fig. 4 we show the activation energy dependence on h at fixed ℓ, which is more relevant to experiment.

B. Bulk magnetostatic energy contribution

We can now go back and check whether the contribution of the bulk magnetostatic term is small compared to the bending energy. This requires an evaluation, or at least an estimate, of the $H^{-1/2}$ Sobolev norm of the divergence of the reduced (i.e., in-plane) magnetization. To do this, we need to introduce some additional notation. The $L^2(\omega)$ norm of a quantity (say, the gradient of the reduced magnetization) is

$$\|\nabla \mathbf{m}\|_{L^2(\omega)} = \left[\int_\omega d^2x (\nabla \mathbf{m})^2\right]^{1/2} \tag{14}$$

so that the dimensionless bending energy is simply $kl^2\|\nabla \mathbf{m}\|^2_{L^2(\omega)}$. From here on we shall abbreviate $L^2(\omega)$ to L^2 for ease of notation.

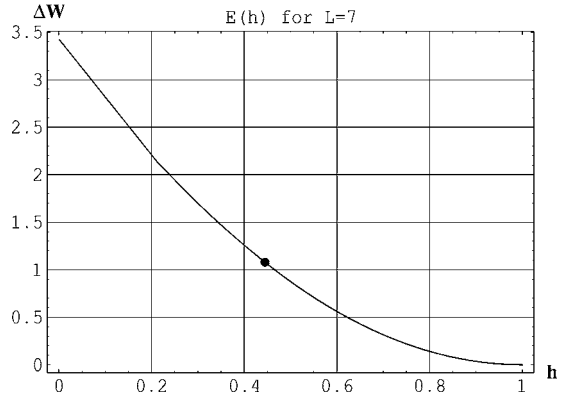

FIG. 4. Activation energy ΔW for fixed $\ell=7$ as h varies. The dot indicates the transition from instanton to constant saddle configuration.

Formally, the $H^{-1/2}$ Sobolev norm of the magnetization divergence is given by[20]

$$\|\nabla \cdot \mathbf{m}\|_{H^{-1/2}} = \|(\nabla)^{-1/2}(\nabla \cdot \mathbf{m})\|_{L^2}. \tag{15}$$

Its meaning becomes clearer through the use of Fourier transforms. Define the Fourier transform $\hat{f}(\xi)$ of $f(\mathbf{x})$ in the usual way: $f(\mathbf{x}) = \int d^2\xi \hat{f}(\xi) e^{i\xi\cdot\mathbf{x}}$. Then

$$\|\nabla \cdot \mathbf{m}\|^2_{H^{-1/2}} = \int d^2\xi \left(\frac{\xi_1 \hat{m}_1 + \xi_2 \hat{m}_2}{|\xi|^{1/2}}\right)^2 = \int d^2\xi \frac{(\xi_1 \hat{m}_1 + \xi_2 \hat{m}_2)^2}{|\xi|}. \tag{16}$$

It now follows in a straightforward fashion that

$$\|\nabla \cdot \mathbf{m}\|_{H^{-1/2}} \leqslant \|\mathbf{m}\|_{H^{1/2}} \leqslant \|\mathbf{m}\|^{1/2}_{L^2} \|\nabla \mathbf{m}\|^{1/2}_{L^2} \leqslant \|\nabla \mathbf{m}\|^{1/2}_{L^2}, \tag{17}$$

where the last inequality follows because $\|\mathbf{m}\|_{L^2}=1$. Therefore the bulk magnetostatic term is dominated by the bending energy.

As noted earlier, the relevant scaling regime for the approach presented here corresponds to $\ell^2 \sim k|\ln k| \sim 10^{-2}-10^{-1}$. For the constant saddle configuration the maximal bulk magnetostatic energy arises when $\phi_u = \pi/2$; this is also the maximum value of ϕ for the saddle, corresponding to $h=0$. For this configuration, and with ring parameters used in Fig. 7, an upper bound for the magnetostatic bulk energy, computed using the inequalities (17), is roughly an order of magnitude smaller than the bending energy. As h increases from 0, and correspondingly $\phi_u \to \pi$, the magnetostatic bulk term decreases to zero.

For the nonconstant, or instanton, saddle, the minimum value of ℓ is 2π. At this length scale, an upper bound for the ratio of magnetostatic bulk energy to bending energy varies roughly from 0.05 to 0.1 as h varies; smaller numbers are found as length scale increases, justifying the neglect of this term.

Qualitatively, the instanton configuration has nonzero divergence only over a region of $O(\delta)$, which remains smaller than $O(1)$ except close to $m=1$ $(\ell \to \infty)$ and $h=1$. The instanton configuration contributes to the bending energy, however, over the entire ring. It is therefore not surprising that, in the appropriate scaling region, the instanton's magnetostatic bulk energy is relatively small compared to its bending energy. This is in contrast to instanton configurations in the cylinder;[5,10] there, while the region contributing to a bulk divergence is $O(1)$, the same region supplies the entire contribution to the bending energy as well, and so the magnetostatic contribution cannot be neglected there.

C. Rate prefactor

The leading-order rate asymptotics are determined by the activation barrier ΔW; the *subdominant* asymptotics appear as the rate prefactor Γ_0. Because the magnitude of Γ_0 is controlled by the extent of fluctuations about the optimal escape path, the prefactor is considerably more difficult to calculate than ΔW. Although the reversal rate is only linearly dependent on the prefactor, as opposed to its exponential

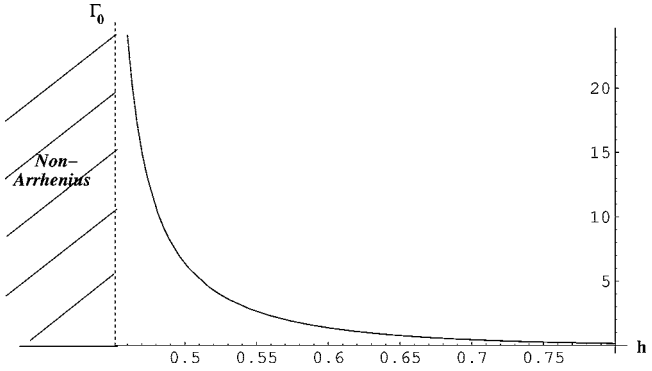

FIG. 5. The prefactor Γ_0 (in units of τ_0^{-1}) vs h when $\ell=7$ on the "constant saddle" side of the transition. The prefactor on the "instanton saddle" side of the transition acquires an additional temperature dependence, as discussed in the text.

dependence on the activation barrier, the rate can still be significantly affected by Γ_0, especially in the vicinity of a transition in saddle configurations (cf. Fig. 5). Moreover, an understanding of the prefactor is needed to study other quantities of physical interest, such as exit location distributions.[27]

The prefactor computation procedure is summarized in Refs. 24 and 28 (see also Refs. 29 and 30). Consider a small perturbation η about the metastable state, so that sufficiently close to it $\phi=\phi_s+\eta$. Then to leading order the time dependence of fluctuations about the metastable state is given by $\dot{\eta}=-\mathbf{\Lambda_s}\eta$, where $\mathbf{\Lambda_s}$ is the linearized zero-noise dynamics at ϕ_s. Similarly $\mathbf{\Lambda_u}$ is the linearized zero-noise dynamics around ϕ_u. Then[24,28]

$$\Gamma_0 = \frac{1}{2\pi}\sqrt{\left|\frac{\det \mathbf{\Lambda_s}}{\det \mathbf{\Lambda_u}}\right|}\,|\lambda_{u,0}|, \tag{18}$$

where $\lambda_{u,0}$ is the single negative eigenvalue of $\mathbf{\Lambda_u}$. Its corresponding eigenvector is the direction along which the optimal escape trajectory approaches the transition state. In general, the determinants in the numerator and denominator of Eq. (18) can separately diverge: they are typically products of an infinite number of eigenvalues with magnitude greater than 1. However, their *ratio*, which can be interpreted as the limit of a product of individual eigenvalue quotients, is finite.

1. Constant saddle

When $\ell<\ell_c(h)$, or equivalently $h>h_c(\ell)$, the saddle is the pair of constant configurations $\phi=\cos^{-1}(-h)$, the prefactor can be determined by direct computation of eigenvalues of the stable and unstable states.[16] Linearizing around the stable state gives

$$\dot{\eta} = -\mathbf{\Lambda_s}\eta = -(-d^2/dx^2 + 1 - h)\,\eta, \tag{19}$$

and similarly

$$\dot{\eta} = -\mathbf{\Lambda_u}\eta = -(-d^2/dx^2 + h^2 - 1)\,\eta \tag{20}$$

about the transition state. The spectrum of eigenvalues corresponding to $\mathbf{\Lambda_s}$ is

$$\lambda_n^s = \frac{4\pi^2 n^2}{\ell^2} + 1 - h, \quad n = 0, \pm 1, \pm 2\ldots \tag{21}$$

and the eigenvalues corresponding to $\mathbf{\Lambda_u}$ are

$$\lambda_n^u = \frac{4\pi^2 n^2}{\ell^2} + h^2 - 1, \quad n = 0, \pm 1, \pm 2\ldots. \tag{22}$$

This simple linear stability analysis justifies the claims that ϕ_s is a stable state and ϕ_u a saddle. Over the interval $[0,\ell_c)$ all eigenvalues of $\mathbf{\Lambda_s}$ are positive, while all but one of $\mathbf{\Lambda_u}$ are. Its single negative eigenvalue $\lambda_0^u=-(1-h^2)$ depends on h but is independent of ℓ.

Putting everything together, we find

$$\Gamma_0^- = \tau_0^{-1}\frac{(1-h^2)}{\pi}\frac{\sinh(\sqrt{1-h}\,\ell/2)}{\sin(\sqrt{1-h^2}\,\ell/2)}, \tag{23}$$

where $\tau_0^{-1}=\alpha\gamma E_0/M_0\mathcal{V}(1+\alpha^2)$, with $\mathcal{V}$ the ring volume. The rate includes a factor of 2 because the system can escape over either of the saddles, which are rotationally equivalent with respect to $\phi_s=\pi$.

The prefactor Γ_0^- diverges at $\ell_c(h)$, or conversely $h_c(\ell)$, as expected (cf. Fig. 5); in this limit, $\Gamma_0^-\sim\text{const}\times(\ell_c-\ell)^{-1}$ as $\ell\to\ell_c^-$ at fixed h, or as $(h-h_c)^{-1}$ as $h\to h_c^+$ at fixed ℓ. The prefactor in this region for fixed ℓ as h varies is plotted in Fig. 5. The divergence arises from the vanishing of the eigenvalue of a pair of degenerate eigenfunctions at the critical point. This indicates the appearance of a pair of soft modes, resulting in a transverse instability of the optimal escape trajectory as it approaches the saddle. The meaning and interpretation of the divergence is discussed in detail in Ref. 16. Near (but not at) the critical point the prefactor formulas hold, but in a vanishing range of T as ℓ_c is approached. Exactly at ℓ_c the prefactor is finite but non-Arrhenius [with a different exponent than that in Eq. (30)]. Inclusion of higher-order fluctuations[31] about the saddle can be used to compute the prefactor at criticality, and will be addressed elsewhere. We return to the prefactor divergence in Sec. VI.

The independence of Γ_0 with respect to temperature leads to the well-known exponential temperature dependence of the overall reversal rate. By analogy with chemical kinetics, this exponential falloff of the rate is often called "Arrhenius behavior."

2. Nonconstant (instanton) saddle

Computation of the determinant quotient in Eq. (18) is less straightforward when the transition state is nonconstant, i.e., when $\ell>\ell_c(h)$ or equivalently $h<h_c(\ell)$. An additional complication follows from the translational degeneracy (energy invariance with respect to choice of s_0) of the nonconstant state. This implies a soft collective mode in the linearized dynamical operator $\mathbf{\Lambda_u}$ of Eq. (18), resulting in a zero eigenvalue for all $h<h_c(\ell)$ [not to be confused with the vanishing of the lowest stable eigenvalue of the saddles exactly at $h_c(\ell)$].

To proceed, we use the McKane-Tarlie regularization procedure,[32] which allows the evaluation of $\det'\mathbf{\Lambda_u}$, the functional determinant of the operator $\mathbf{\Lambda_u}$ with the zero ei-

genvalue removed. We refer the reader to Ref. 32 for details, but sketch the main features here.

With periodic boundary conditions, it is formally the case that

$$\frac{\det' \mathbf{\Lambda_u}}{\langle \eta_1 | \eta_1 \rangle} = \frac{\eta_2(s+\ell, s_0; m) - \eta_2(s, s_0; m)}{\eta_1(s, s_0; m) \det \mathbf{H}(s, s_0; m)}, \tag{24}$$

where $\eta_1(s, s_0; m)$ and $\eta_2(s, s_0; m)$ are two linearly independent solutions of $\mathbf{\Lambda_u}\eta_i = 0$, $i = 1, 2$, $\langle \eta_1 | \eta_1 \rangle = \int_{-\ell/2}^{\ell/2} ds y_1^2(s, 0; m)$ is the square of the norm of the zero mode, and $\det \mathbf{H}(s, s_0; m) = \dot{\eta}_2(s, s_0; m)\eta_1(s, s_0; m) - \dot{\eta}_1(s, s_0; m)\eta_2(s, s_0; m)$ is the Wronskian; here a dot denotes a derivative with respect to s. The expression (24) is meaningful only as part of a determinant quotient, as noted above.

The functions η_1 and η_2 can be found by differentiating the instanton solution (8) with respect to s_0 and m, respectively; i.e., $\eta_1(s, s_0; m) = \partial\phi(s, s_0; m)/\partial s_0$ and $\eta_2(s, s_0; m) = \partial\phi(s, s_0; m)/\partial m$. This yields

$$\eta_1(s, s_0; m) = -\frac{2m}{\delta} \mathrm{sn}(\mathcal{R}|m)\mathrm{cn}(\mathcal{R}|m) \times \frac{\mathrm{sn}\left(\frac{s-s_0}{\delta}|m\right)\mathrm{cn}\left(\frac{s-s_0}{\delta}|m\right)}{\mathrm{cn}^2(\mathcal{R}|m) + \mathrm{sn}^2(\mathcal{R}|m)\mathrm{dn}^2\left(\frac{s-s_0}{\delta}|m\right)} \tag{25}$$

and

$$\begin{aligned}\eta_2(s, s_0; m) = &-\frac{2}{\mathrm{cn}^2(\mathcal{R}|m) + \mathrm{sn}^2(\mathcal{R}|m)\mathrm{dn}^2\left(\frac{s-s_0}{\delta}|m\right)} \\ &\times \left\{ \frac{m(s-s_0)}{\delta^2}\frac{d\delta}{dm}\mathrm{sn}(\mathcal{R}|m)\mathrm{cn}(\mathcal{R}|m)\mathrm{sn}\left(\frac{s-s_0}{\delta}|m\right)\mathrm{cn}\left(\frac{s-s_0}{\delta}|m\right) \right. \\ &+ \frac{\mathrm{sn}(\mathcal{R}|m)\mathrm{cn}(\mathcal{R}|m)}{2(1-m)}\left[\mathrm{sn}\left(\frac{s-s_0}{\delta}|m\right)\mathrm{cn}\left(\frac{s-s_0}{\delta}|m\right)E\left(\frac{s-s_0}{\delta}|m\right) - \mathrm{sn}\left(\frac{s-s_0}{\delta}|m\right)\mathrm{cn}\left(\frac{s-s_0}{\delta}|m\right)(1-m)\left(\frac{s-s_0}{\delta}\right) \right. \\ &\left. \left. - \mathrm{sn}^2\left(\frac{s-s_0}{\delta}|m\right)\mathrm{dn}\left(\frac{s-s_0}{\delta}|m\right)\right] + \mathrm{dn}(\mathcal{R}|m)\frac{d\mathcal{R}}{dm}\mathrm{dn}\left(\frac{s-s_0}{\delta}|m\right) \right\}, \end{aligned} \tag{26}$$

where $\mathbf{E}(\cdot|m)$ is the incomplete elliptic integral of the second kind.[26]

Inserting these solutions into Eq. (24) yields

$$\left| \frac{\det' \mathbf{\Lambda_u}}{\langle \eta_1 | \eta_1 \rangle} \right| = \frac{\delta^3[(2m/\delta)(d\delta/dm)\mathbf{K}(m) - \mathbf{K}(m) + \mathbf{E}(m)/(1-m)]}{4m^2 \mathrm{sn}(\mathcal{R}|m)\mathrm{cn}(\mathcal{R}|m)\mathrm{dn}(\mathcal{R}|m)d\mathcal{R}/dm}. \tag{27}$$

Using a similar procedure, we find the corresponding numerator for the determinant ratio in Eq. (18) to be

$$\det \mathbf{\Lambda_s} = 4 \sinh^2[\delta\sqrt{1-h}\mathbf{K}(m)], \tag{28}$$

consistent with the numerator of Eq. (23), obtained through direct computation of the eigenvalue spectrum. (Recall, though, that it is only the *ratio* of the determinants that is sensible.) This becomes clearer by noting that the expressions in Eqs. (27) and (28) are well behaved for all finite $\ell > \ell_c$ ($m > 0$). While both expressions separately diverge as $m \to 1$, it is easily checked that the divergences cancel.

As already noted, the rotational symmetry of the instanton state (corresponding to the arbitrariness of the constant s_0) corresponds to a "soft mode," resulting in appearance of a zero eigenvalue $\lambda_{u,1} = 0$ of the operator $\mathbf{\Lambda_u}$. The corresponding eigenfunction is clearly η_1 given by Eq. (25). The appearance of a zero mode corresponds to the zero rotational energy of the instanton solution: the center of the domain wall pair can appear anywhere in the ring. This is in contrast

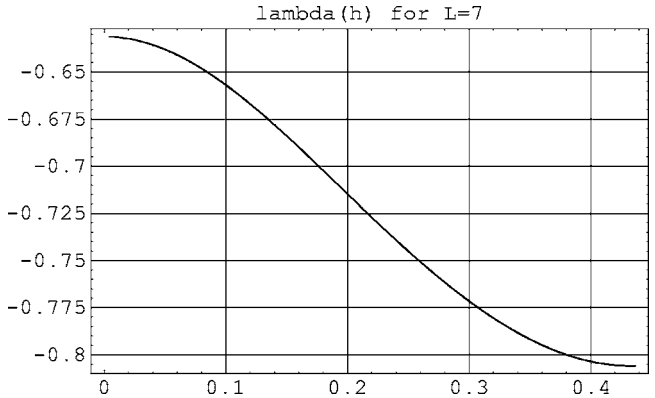

FIG. 6. Lowest eigenvalue $\lambda_{u,0}$ as a function of h for $\ell = 7$.

to the situation in the finite cylinder,[25] where the instanton is "pinned." The general procedure for including the correction required due to removal of the zero eigenvalue is described by Schulman.[30] The correction in our problem is an additional factor of $2\ell\sqrt{\langle\eta_1|\eta_1\rangle/\pi k_B T}$, which vanishes as $m\to 0$ (and thereby removes the divergence of the prefactor as $m\to 0^+$).

Finally, we need to compute the eigenvalue $\lambda_{u,0}$ corresponding to the unstable direction. With the substitution $z=(s-s_0)/\delta$, the eigenvalue equation $\mathbf{\Lambda_u}\eta=\lambda\eta$ becomes

$$0=\frac{d^2\eta}{dz^2}+\delta^2\eta\times\left\{\frac{(\lambda+1-h)\mathrm{cn}^4(\mathcal{R}|m)+2(\lambda+3)\mathrm{sn}^2(\mathcal{R}|m)\mathrm{cn}^2(\mathcal{R}|m)\mathrm{dn}^2(z|m)+(\lambda-1-h)\mathrm{sn}^4(\mathcal{R}|m)\mathrm{dn}^4(z|m)}{[\mathrm{cn}^2(\mathcal{R}|m)+\mathrm{sn}^2(\mathcal{R}|m)\mathrm{dn}^2(z|m)]^2}\right\}. \quad (29)$$

The lowest eigenvalue corresponds to a nodeless solution for η. By continuity it must tend towards $-1+h^2$ as $m\to 0^+$. We have solved Eq. (29) numerically for $\ell=7$; the result appears in Fig. 6. The weak dependence on h (and also ℓ) is typical.

Finally, we put all of the above results together to find the formula for the prefactor *per unit length*:

$$\tau_0\Gamma_0^+/\ell=|\lambda_0(\ell,h)|m(k_BT)^{-1/2}\sinh[\delta\sqrt{1-h}\mathbf{K}(m)]\times\left(2m\mathbf{K}(m)\frac{d\ln\delta}{dm}+\frac{1}{1-m}\times[\mathbf{E}(m)-(1-m)\mathbf{K}(m)]\right)^{-1/2}, \quad (30)$$

where $\mathbf{E}(m)$ is the complete elliptic function of the second kind.[26] As noted above, $\lambda_0(\ell,h)$ is weakly dependent on h and ℓ, and is $O(1)$ everywhere.

The most important qualitative feature to be noted from Eq. (30) is that the zero eigenvalue arising from the uniform translation mode leads to non-Arrhenius behavior—i.e., a T-dependent prefactor—everywhere on the low-field side of the transition.

Finally, we note that the eigenfunction η_1 given by Eq. (25) has a single pair of nodes. Because nodes arise in pairs, there must then be only a single (nodeless) solution of lower eigenvalue than η_1. But η_1 has zero eigenvalue, proving that the solution (8) has a single unstable eigenmode, and is therefore a proper saddle.

The above results allow one to find the overall reversal rate in any part of the (ℓ,h) phase plane. Results for a permalloy ring with given dimensions are shown in Fig. 7.

Among commonly used soft ferromagnetic materials, permalloy has the largest magnetic exchange length. The discussion of scaling in Sec. III suggests that the effects of nonlocal magnetostatic terms are minimized with larger exchange lengths. Where else might one find magnetic materials with large exchange lengths? Such materials would require both low magnetization density and large exchange constants. This combination occurs naturally in certain ferrimagnets. One example is $MgOFe_2O_3$, which has an exchange length a factor of 5 larger than that of permalloy. There are many examples of such materials that have been prepared as polycrystalline thin films, and thus are soft magnets (i.e., have no or very weak magnetocrystalline anisotropies). Such materials might prove useful for experimental studies of the phenomena described in this paper.

VI. DISCUSSION

A theory of magnetization reversal in thin micromagnetic rings has been presented. Such systems are distinguished by their lack of edges or corners where nucleation is easily initiated, leading to greater stability of magnetization configurations and facilitating comparison of theory to experiment.

By utilizing a scaling analysis[19] that uncovers a separation of energy scales in the thin-film limit, we are able to retain

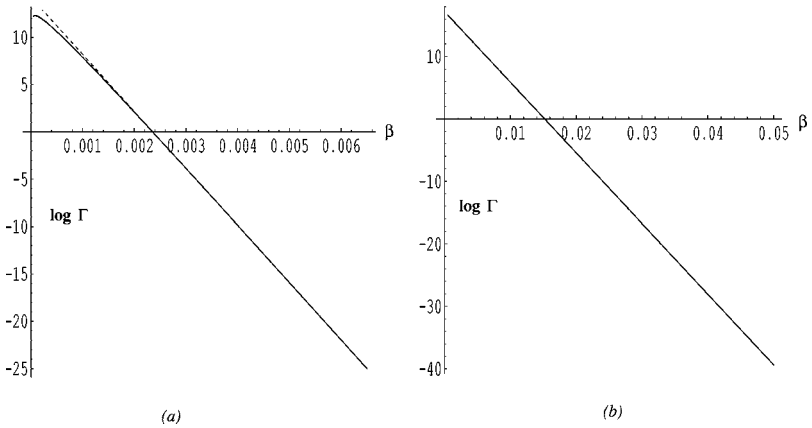

FIG. 7. Total switching rate (in units of s^{-1}) vs $\beta=1/k_BT$ (in units of K^{-1}), at fields of (a) 60 mT (instanton saddle) and (b) 72 mT (constant saddle). Parameters used are $k=0.01$, $l=0.1$, $R=200$ nm, $R_1=180$ nm, $R_2=220$ nm, $M_0=8\times10^5$ A/m (permalloy), $\alpha=0.01$, and $\gamma=1.7\times10^{11}$ T^{-1} s^{-1}. Deviation of low-field switching rate in (a) from dashed line signals non-Arrhenius behavior.

leading-order terms that allow for an analytic solution of the relevant magnetization configurations in the thermally induced reversal problem. The discarded terms, in particular those corresponding to nonlocal magnetostatic energy contributions, are shown to contribute no more than $O(10\%)$ to the energy over most values in the (ℓ,h) phase plane. A complete solution that takes into account all terms must be numerical, and is planned for future work.

Nevertheless, an analytic solution is highly useful and can uncover information that may be difficult to extract from a numerical one. In particular, we predict an unusual transition from Arrhenius to non-Arrhenius activation behavior (cf. Fig. 7). Our analysis suggests that such a transition should now be observable experimentally, by varying the externally applied magnetic field for rings of fixed size. A clear signature of such a transition would be the observation of a crossover from Arrhenius to non-Arrhenius behavior as field varies, as seen in Fig. 7. Because this requires measurement of the prefactor, such an observation would require numerous runs where reversal occurs.

Arrhenius behavior of magnetic reversal has already been found in several systems and geometries. In Ref. 4, measurements of switching field and waiting times on nearly spherical Ni, Co, and Dy nanoparticles found an activation volume close to the particle volume, indicating a uniform magnetization reversal (analogous to the constant saddle case here) and confirming the Néel-Brown theory for these systems. In contrast, measurements on Ni wires with diameters 40–100 nm revealed an activation volume considerably smaller than the particle volume, indicating a nonuniform transition state (analogous to our instanton saddle). Here, too, Arrhenius switching behavior was found. But would not the arguments given above imply that one should see non-Arrhenius behavior for these wires? No, because here the (roughly) cylindrical geometry with end caps (and consequently the relevant boundary conditions on the magnetization), lead to the absence of a uniform translation or rotational symmetry present, and therefore no zero mode leading to a temperature-dependent prefactor. In fact, these observations support the robustness of our conclusions for a wider variety of cases than considered in this paper. We will discuss this further below.

Before doing that, however, we wish to suggest a second experimental test that may be easier to conduct: this is to measure the dependence of the activation energy on mean radius R for rings of identical composition. On the Arrhenius side of the transition, where magnetization reversal proceeds via a uniform rotation of the magnetization, the activation barrier scales linearly with the ring size. However, on the non-Arrhenius side, where the instanton state governs the reversal, the activation barrier is almost independent of ring size (see Fig. 3). In this set of measurements, one may need to alter the applied field as ring size varies to keep the system on one or the other side of the transition, given that the critical field depends on R [cf. Eq. (12)].

How robust are our predictions of a transition in activation behavior, and in particular, can the neglected energy contributions wash out or obscure the transition? It is indeed possible, perhaps likely, that the details of the transition close to the critical field (or circumference if field is fixed) are sensitive to these terms. In particular, the second-order nature of the transition, and the corresponding divergence of the prefactor (cf. Fig. 5), could disappear. Inclusion of the magnetostatic terms could even in principle change the transition from second- to first-order, with a jump replacing the divergence in the prefactor. Such first-order transitions have been predicted to occur in thermally induced conductance jumps in monovalent metallic nanowires.[33]

However, our central prediction, a transition from Arrhenius to non-Arrhenius activation behavior, should be robust because it is due to something much more fundamental: a rotationally invariant transition state [our "constant" state $\phi=\cos^{-1}(-h)$] at high fields and a rotationally noninvariant state [our instanton state (8)] at low fields, with the crossover determined primarily through a competition between the shape anisotropy arising from magnetostatic forces and the Zeeman energy arising from the external field. In fact, the discussion in Sec. V C 2 leads to the conclusion that the appearance at lower fields of *any* rotationally noninvariant state should give non-Arrhenius switching behavior in the ring geometry. Experimentally, what is then required is a symmetric enough ring so that the "domain wall" part of the transition state (centered at s_0 in our instanton solution) has more or less equal probability of nucleating anyplace along the ring. This "Goldstone mode," arising from the rotationally invariant geometry, is ultimately where the non-Arrhenius factor comes from. Although the size constraints on the ring parameters leading to the specific instanton solution (8) are difficult to realize at the present time, the generality of the basic physical features determining the transition should lead to the predicted crossover from Arrhenius to non-Arrhenius behavior in at least some ring geometries that are outside of the scaling regime considered here.

ACKNOWLEDGMENTS

This research was partially supported by NSF Grant Nos. PHY-0351964 (D.L.S.), FRG-DMS-0101439 and DMR-0405620 (A.D.K.), and the Akademisches Auslands Amt and the Evangelisches Studienwerk e.V. Villigst (K.M.). K.M. thanks the Physics Department of the University of Arizona for their hospitality and support during her stay. D.L.S. thanks Bob Kohn and Valeriy Slastikov for numerous valuable discussions, and for providing several references.

*Present address: Institut für Theoretische Physik, Universität Heidelberg, Philosophenweg 19, 69120 Heidelberg, Germany.

†Present address: Department of Physics and Courant Institute of Mathematical Sciences, New York, NY 10003.

[1] F. H. deLeeuw, R. van den Doel, and U. Enz, Rep. Prog. Phys. **43**, 689 (1980).

[2] L. Néel, Ann. Geophys. (C.N.R.S.) (C.N.R.S.) **5**, 99 (1949).

[3] W. F. Brown, Jr., Phys. Rev. **130**, 1677 (1963).

[4] W. Wernsdorfer, E. B. Orozco, K. Hasselbach, A. Benoit, B. Barbara, N. Demoncy, A. Loiseau, H. Pascard, and D. Mailly, Phys. Rev. Lett. **78**, 1791 (1997).
[5] H.-B. Braun, Phys. Rev. Lett. **71**, 3557 (1993).
[6] G. Brown, M. Novotny, and P. A. Rikvold, J. Appl. Phys. **87**, 4792 (2001).
[7] E. D. Boerner and H. N. Bertram, IEEE Trans. Magn. **34**, 1678 (1998).
[8] Z. Li and S. Zhang, Phys. Rev. B **69**, 134416 (2004).
[9] W. Wernsdorfer, B. Doudin, D. Mailly, K. Hasselbach, A. Benoit, J. Meier, J.-P. Ansermet, and B. Barbara, Phys. Rev. Lett. **77**, 1873 (1996).
[10] A. Aharoni, J. Appl. Phys. **80**, 3133 (1996).
[11] W. E, W. Ren, and E. Vanden-Eijnden, J. Appl. Phys. **93**, 2275 (2003).
[12] Both of these issues are addressed in H.-B. Braun, J. Appl. Phys. **85**, 6172 (1999).
[13] J. G. Zhu, Y. Zheng, and G. A. Prinz, J. Appl. Phys. **87**, 6668 (2000).
[14] J. Rothman, M. Klaui, L. Lopez-Diaz, C. A. F. Vaz, A. Bleloch, J. A. C. Bland, and Z. Cui, Phys. Rev. Lett. **86**, 1098 (2001).
[15] R. S. Maier and D. L. Stein, Phys. Rev. Lett. **87**, 270601 (2001).
[16] D. L. Stein, J. Stat. Phys. **114**, 1537 (2004).
[17] K. Martens, D. L. Stein, and A. D. Kent, in *Noise in Complex Systems and Stochastic Dynamics III*, edited by L. Kish, K. Lindenberg, and Z. Gingl (SPIE, Bellingham, 2005), pp. 1–11.
[18] A. Aharoni, *Introduction to the Theory of Ferromagnetism* (Oxford University Press, Oxford, 2000), 2nd ed.
[19] R. V. Kohn and V. V. Slastikov, Arch. Ration. Mech. Anal. (to be published).
[20] A. DeSimone, R. V. Kohn, S. Muller, and F. Otto, Commun. Pure Appl. Math. **55**, 1408 (2002).
[21] The magnetostatic energy also contains a mixing term between bulk and boundary contributions, which scales the same as the bulk term; it is therefore omitted here. Its contribution is the same order as that of the bulk term, which is shown in the text to be at least an order of magnitude smaller than all of the other terms.
[22] T. Shinjo, T. Okuno, R. Hassdorf, K. Shigeto, and T. Ono, Science **289**, 930 (2000).
[23] N. A. Usov and S. E. Pechany, J. Magn. Magn. Mater. **118**, L290 (1993).
[24] P. Hänggi, P. Talkner, and M. Borkovec, Rev. Mod. Phys. **62**, 251 (1990).
[25] R. S. Maier, in *Noise in Complex Systems and Stochastic Dynamics II*, edited by Z. Gingl, J. M. Sancho, L. Schimansky-Geier, and J. Kertesz (SPIE, Bellingham, 2004), pp. 48–57, independently found a spatially varying solution for finite cylindrical geometries.
[26] M. Abramowitz and I. A. Stegun, eds., *Handbook of Mathematical Functions* (Dover, New York, 1965).
[27] R. S. Maier and D. L. Stein, SIAM J. Appl. Math. **57**, 752 (1997).
[28] F. Moss and P. V. E. McClintock, eds., *Noise in Nonlinear Dynamical Systems* (Cambridge University Press, Cambridge, England, 1989), three volumes.
[29] J. S. Langer, Ann. Phys. (N.Y.) **41**, 108 (1967).
[30] L. S. Schulman, *Techniques and Applications of Path Integration* (Wiley, New York, 1981).
[31] M. Reznikoff, Ph.D. thesis, New York University, New York, 2004, p. 166, addresses some of the mathematical issues surrounding the breakdown of the harmonic approximation (used in the prefactor calculation) due to the existence of an exponentially small eigenvalue at the critical point.
[32] A. J. McKane and M. B. Tarlie, J. Phys. A **28**, 6931 (1995).
[33] J. Bürki, C. A. Stafford, and D. L. Stein, Phys. Rev. Lett. **95**, 090601 (2005).